Coexistence of antiferromagnetic order and unconventional superconductivity in heavy-fermion CeRh$_{1-x}$Ir$_x$In$_5$ compounds: Nuclear quadrupole resonance studies

Guo-qing Zheng,[1,]* N. Yamaguchi,[1] H. Kan,[1] Y. Kitaoka,[1] J. L. Sarrao,[2] P. G. Pagliuso,[2] N. O. Moreno,[2] and J. D. Thompson[2]

[1]*Department of Physical Science, Graduate School of Engineering Science, Osaka University, Osaka 560-8531, Japan*

[2]*Condensed Matter and Thermal Physics, MS K764, Los Alamos National Laboratory, Los Alamos, New Mexico 87545, USA*

We present a systematic ^{115}In NQR study on the heavy-fermion compounds CeRh$_{1-x}$Ir$_x$In$_5$ (x=0.25, 0.35, 0.45, 0.5, 0.55, and 0.75). The results provide strong evidence for the microscopic coexistence of antiferromagnetic (AF) order and superconductivity (SC) in the range of $0.35 \leq x \leq 0.55$. Specifically, for x=0.5, T_N is observed at 3 K with a subsequent onset of superconductivity at T_c=0.9 K. T_c reaches a maximum (0.94 K) at x=0.45 where T_N is found to be the highest (4.0 K). Detailed analysis of the measured spectra indicate that the same electrons participate in both SC and AF order. The nuclear spin-lattice relaxation rate $1/T_1$ shows a broad peak at T_N and follows a T^3 variation below T_c, the latter property indicating unconventional SC as in CeIrIn$_5$ (T_c=0.4 K). We further find that, in the coexistence region, the T^3 dependence of $1/T_1$ is replaced by a T-linear variation below $T \sim 0.4$ K, with the value $(T_1)_{T_c}/(T_1)_{\text{low } T}$ increasing with decreasing x, likely due to low-lying magnetic excitations associated with the coexisting magnetism.

I. INTRODUCTION

Superconductivity and long-range magnetic order are two outstanding quantum phenomena; however, these ground states are not generally displayed by the same electrons simultaneously. This is because an internal magnetic field arising from magnetic order usually destroys superconductivity. In the 1970's, a number of materials were found to host both superconductivity and magnetic order, but the two orders were due to different electrons and occurred in spatially separated regions.[1] This is also true in the recently reported ruthenatecuprate hybrid compound RuSr$_2$$RCu_2O_8$ (R =rare earth) where the RuO and CuO$_2$ planes are responsible for the magnetic order and superconductivity, respectively.[2] An exceptional case is the heavy-fermion compound UPd$_2$Al$_3$ in which magnetic order and superconductivity coexist homogeneously.[3,4] In this system, however, it is believed that the multiple bands of uranium (U) electrons make such coexistence possible. Namely, among three U-5f electrons, the two with localized character are responsible for the magnetism and the remaining one is responsible for superconductivity.[5,6] Such "duality" may also be at work in other U-based heavy-fermion magnetosuperconductors.[7–9] It is therefore an outstanding question whether magnetic order and superconductivity due to the same electrons can coexist on a microscopic length scale. Although it has been proposed theoretically that magnetism and superconductivity may be viewed as two subcomponents of a unified group and that they may coexist under certain conditions,[10] accumulation of convincing experimental evidence is important. The Ce-based heavy-fermion compounds and high superconducting transition-temperature (T_c) copper oxides are hosts of single-band magnetism or/and superconductivity, and are therefore good candidate materials for exploring this problem.

Recently, it has been suggested that in the layered heavy-fermion compounds Ce(Rh$_{1-x}$Ir$_x$)In$_5$ (Ref. 11) and Ce(Rh$_{1-x}$Co$_x$)In$_5$ (Ref. 12) and also CeRhIn$_5$ under pressure,[13,14] antiferromagnetism and superconductivity coexist. CeRh(Ir)In$_5$ crystallizes in a tetragonal structure which consists of CeIn$_3$ layers separated by a Rh(Ir)In$_2$ block. CeRhIn$_5$ is an antiferromagnet with T_N=3.7 K, but becomes superconducting under pressures above 1.6 GPa.[15] CeIrIn$_5$ is a superconductor at ambient pressure with T_c=0.4 K (Ref. 16) and line nodes in the superconducting energy gap.[17] It is remarkable that the magnetic fluctuations exhibit quasi-two-dimensional character as revealed by NQR (Ref. 17) and neutron scattering[18] measurements, probably reflecting the layered crystal structure. Upon substituting Rh with Ir, superconductivity was found in Ce(Rh$_{1-x}$Ir$_x$)In$_5$ for $x > 0.3$, while magnetic order continued to be observed around 3.8 K in the specific heat for $x \leq 0.5$ (Ref. 11) and an internal magnetic field was detected by muon spin rotation measurement.[19]

In this paper, we present results obtained from nuclear quadrupole resonance (NQR) measurements on Ce(Rh$_{1-x}$Ir$_x$)In$_5$ that strongly suggest that antiferromagnetic (AF) order coexists microscopically with unconventional superconductivity (SC). We find that upon replacing Rh with Ir in the antiferromagnet CeRhIn$_5$, the Neel temperature T_N increases slightly with increasing Ir content up to x=0.45 then decreases rapidly. Superconductivity sets in above $x \sim 0.35$ and T_c reaches a maximum of 0.94 K at x=0.45. The nuclear spin-lattice relaxation rate $1/T_1$ shows a broad peak at T_N and follows a T^3 variation below T_c, the latter feature indicating that the SC is unconventional as in CeIrIn$_5$. In the coexistence region, $1/T_1$ becomes proportional to T at very low temperatures in the superconducting state and the value $T_1(T=T_c)/T_1$ increases in the order of x=0.55, 0.5, and 0.45, which suggests the existence of low-lying magnetic excitations in addition to the residual density of states (DOS) due to the presence of disorder.

The rest of the paper is organized as follows. The experimental details are described in Sec. II. In Sec. III, the NQR spectroscopy that indicates the homogeneous alloying of the samples is presented. The results of the nuclear spin lattice

70 014511-1

relaxation that evidence the coexistence of antiferromagnetism and superconductivity are also presented in Sec. III, along with evidence for the unconventional nature of the superconductivity. We conclude in Sec. IV, following a brief discussion of the phase diagram deduced from our NQR measurements.

II. EXPERIMENTAL

Single crystals of $Ce(Rh_{1-x}Ir_x)In_5$ used in this study were grown by the In-flux method.[15] For NQR measurements, the single crystals were crushed into a powder of moderate particle size to allow maximal penetration of the oscillating magnetic field H_1, used in the NQR measurements. The measurements below 1.4 K were performed by using a $^3He/^4He$ dilution refrigerator. NQR experiments were performed using a home-built phase-coherent spectrometer. A standard $\pi/2$-π-echo pulse sequence was used. A small H_1 was used to avoid possible heating by the rf pulse below 1K; the $\pi/2$ pulse length is about 20 microseconds. A CuBe piston-cylinder device,[20] filled with Si-based organic liquid as a pressure-transmitting medium, was used to generate high pressure. The NQR coil was put inside a Teflon cell. To calibrate the pressure at low temperatures, the reduction in T_c of Sn metal under pressure was monitored by resistivity measurements.[21] T_c of the samples was determined from the ac susceptibility measured by using the NQR coil at a frequency of ~ 32 MHz, and from the T_1 data (see below). $1/T_1$ was measured by the saturation-recovery method. The value of $1/T_1$ was unambiguously extracted from a good fitting of the nuclear magnetization to the expected theoretical curve[22,23] (discussed in detail below).

III. RESULTS AND DISCUSSION

A. Evidence for homogeneous alloying from NQR spectra

There are two inequivalent crystallographic sites of In in $Ce(Rh_{1-x}Ir_x)In_5$: the In(1) site in the $CeIn_3$ plane and the In(2) site in the $Rh(Ir)In_2$ block. The NQR spectra for the In(1) site consist of four equally spaced transition lines separated by ν_Q, while the In(2) spectra are composed of four unequally separated lines between 30 and 72 MHz. The spectra of $CeIrIn_5$ (Ref. 17) is reproduced in Fig. 1(a). Here ν_Q is defined as the parameter in the following Hamiltonian:

$$H_Q = \frac{h\nu_Q}{6}\left(3I_z^2 - I(I+1) + \frac{1}{2}\eta(I_+^2 + I_-^2)\right), \quad (1)$$

where

$$\nu_Q = \frac{eQV_{zz}}{6I(2I+1)} \quad (2)$$

and

$$\eta = \frac{V_{xx} - V_{yy}}{V_{zz}}. \quad (3)$$

A representative spectra for $CeRh_{0.5}Ir_{0.5}In_5$ is shown in Fig. 1(b). Two effects due to alloying are readily seen in this
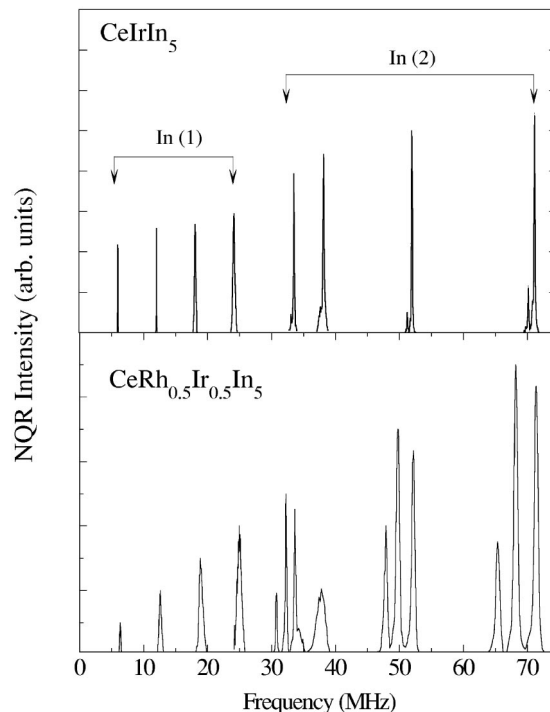

FIG. 1. ^{115}In NQR spectra at $T=4.2$ K for $CeIrIn_5$ [upper panel (Ref. 17)], and for $CeRh_{0.5}Ir_{0.5}In_5$ (lower panel).

spectra. First, the transition lines for In(1) are broadened. Second, each transition for In(2) is split into three lines. Although naively this behavior might suggest phase segregation, we argue below by inspecting the Ir-concentration dependence of the spectra, that there is no phase separation in the alloyed sample; rather the sample is globally homogeneous.

Figure 2 shows the NQR line shape at $T=4.2$ K of the $2\nu_Q$ transition at the In(1) site for various Ir contents. The ν_Q decreases monotonically from 6.78 MHz $(x=0)$[24] to 6.065 MHz $(x=1)$,[17] suggesting a smooth evolution of the lattice upon alloying, in agreement with x-ray diffraction measurements.[11] It should be emphasized that no trace of pure $CeRhIn_5$ or $CeIrIn_5$ is found in the alloyed samples because no peaks corresponding to $x=0$ or $x=1$ were observed.

Figure 3 shows the spectra corresponding to the lowest transition $(m=\pm3/2\leftrightarrow\pm5/2)$ line of the In(2) site for various Ir concentration ranging from $x=0.25$ to 0.75. It is interesting that the positions of the three peaks do not change with Ir concentration [Fig. 4(a)], but the relative intensity distribution among these lines does [Fig. 4(b)]. Also, the left peak is at the same position of the $m=\pm3/2\leftrightarrow\pm5/2$ transition for $CeRhIn_5$, while the right peak is at the same position as the corresponding transition for pure $CeIrIn_5$. The central peak is characterized by $\nu_Q=17.37$ MHz and $\eta=0.473$.

Figure 4(c) depicts a quantity that is the relative intensity shown in Fig. 4(b) multiplied by the corresponding peak position shown in Fig. 4(a). Most simply, this corresponds to the "weighted peak position" or "averaged resonance frequency" for the $m=\pm3/2\leftrightarrow\pm5/2$ transition. Note that this quantity increases smoothly with increasing Ir concentration.
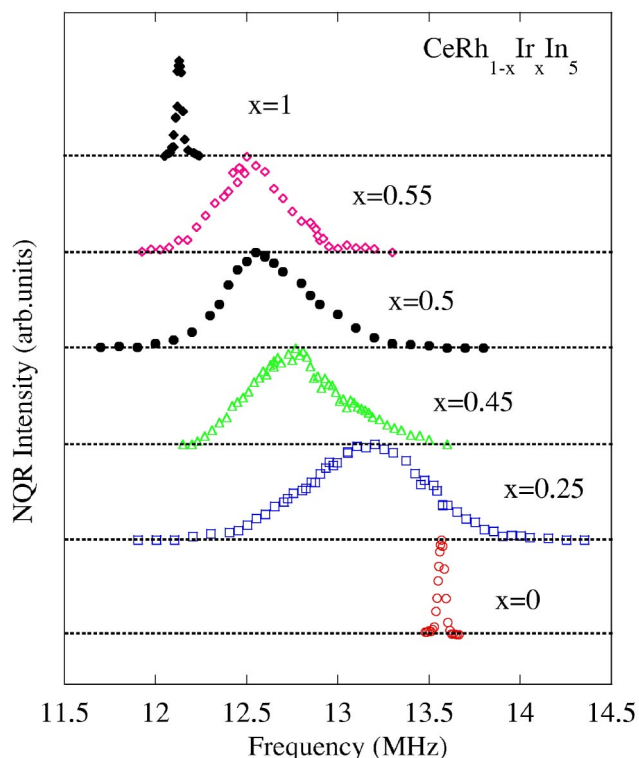
FIG. 2. (Color online) ^{115}In NQR line shape ($\pm 3/2 \leftrightarrow \pm 5/2$ transition) of the In(1) site in $CeRh_{1-x}Ir_xIn_5$ at $T=4.2$ K for various Ir content. The horizontal line under each spectrum is the position of zero intensity for that spectrum.

The results shown in Fig. 4 can be interpreted as follows. In(2) has two nearest-neighbor M (Rh, Ir) sites. There are x Ir atoms and $(1-x)$ Rh atoms for a given alloy concentration x. If the NQR frequency is sensitive to the local environment, there will be three resonance lines depending on the nearest-neighbor configuration of a given In(2), namely, (Rh,
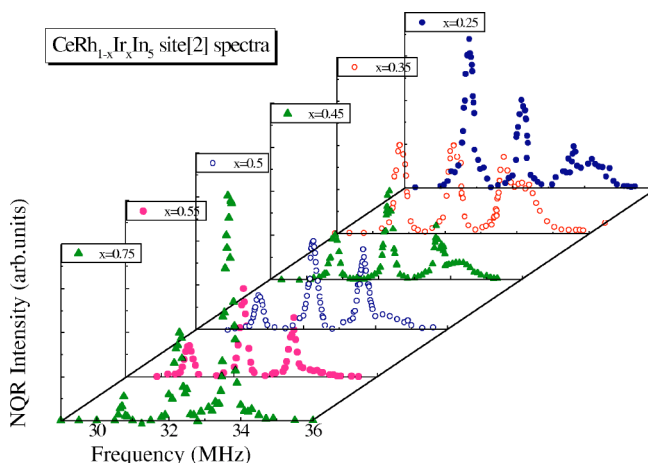

FIG. 3. (Color online) ^{115}In NQR line shape ($\pm 3/2 \leftrightarrow \pm 5/2$ transition) of the In(2) site of $CeRh_{1-x}Ir_xIn_5$ at $T=4.2$ K for various Ir content. In this plot, the vertical axis was adjusted so that all samples have the same height for the central peak (around 32.2 MHz). The signal around 35 MHz for low x is from the second lowest transition($\pm 1/2 \leftrightarrow \pm 3/2$ transition); also see Fig. 1(b).
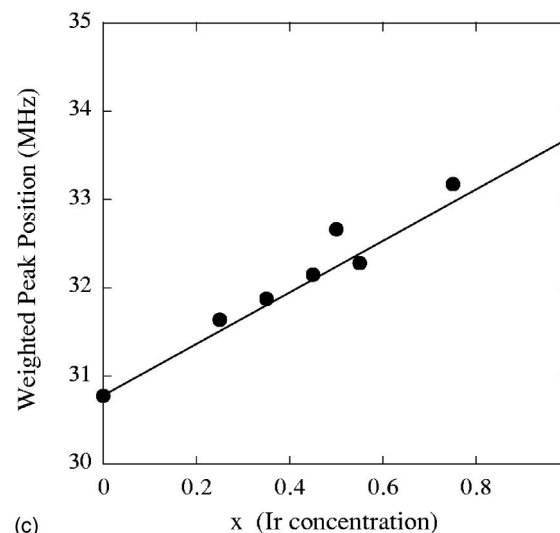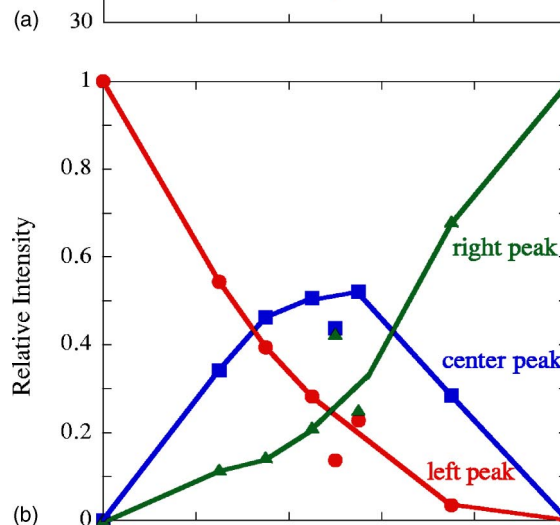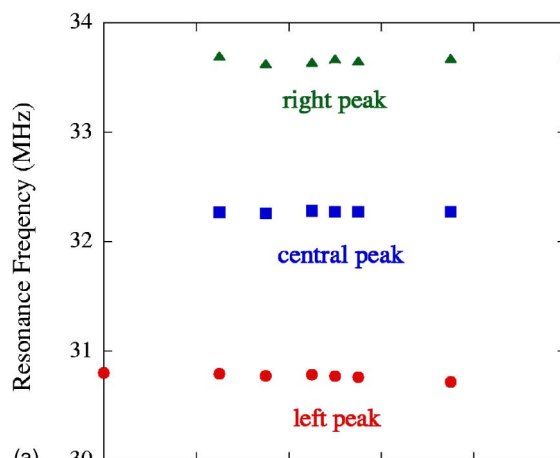

FIG. 4. (Color online) (a) Peak frequency of the three $\pm 3/2 \leftrightarrow \pm 5/2$ transition lines of the In(2) site of $CeRh_{1-x}Ir_xIn_5$ at $T=4.2$ K. (b) Ir-content dependence of the relative intensity of the three $\pm 3/2 \leftrightarrow \pm 5/2$ transition lines of the In(2) site of $CeRh_{1-x}Ir_xIn_5$. (c) Ir-content dependence of the peak frequency multiplied by the relative intensity for the three In(2) $\pm 3/2 \leftrightarrow \pm 5/2$ transition lines.
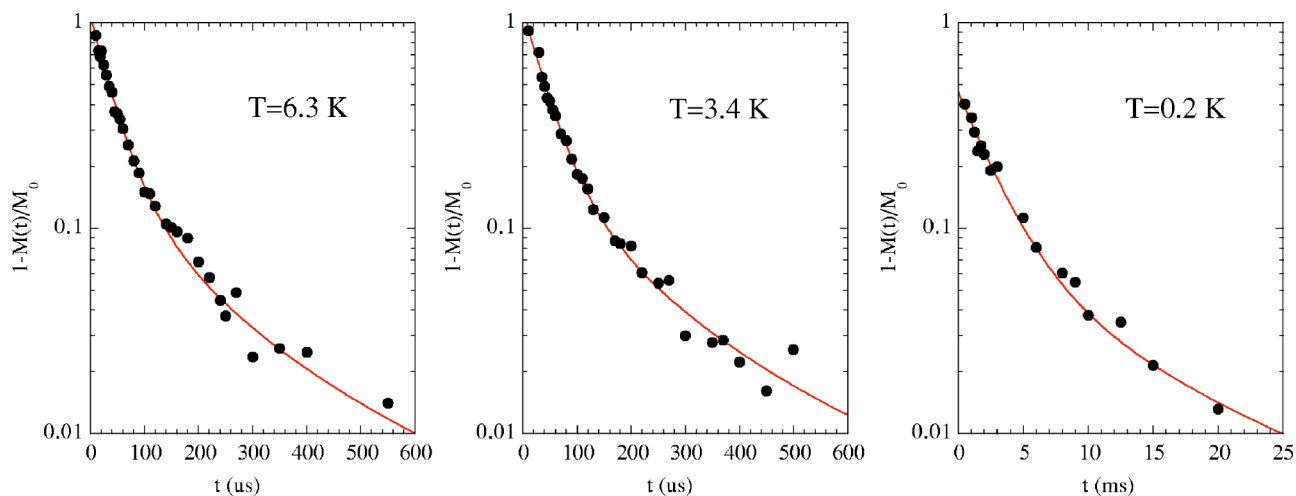
FIG. 5. (Color online) Time dependence of the nuclear magnetization of the In(1) site at various temperatures in $CeRh_{0.55}Ir_{0.45}In_5$. The curves are fitting to Eq. (4) in the text.

Rh), (Rh, Ir), or (Ir,Ir). The intensity of each peak will be proportional to the probability that In(2) has a corresponding nearest neighbor pair, namely, (Rh, Rh), (Rh, Ir), or (Ir,Ir). Figure 4 strongly suggests that this is the case, with the central transition corresponding to the case with (Rh,Ir) nearest neighbors.

In such a scenario, one might then wonder why In(1) only sees an averaged environment. This is probably because the wave function mixing between In(1) and the M atom is
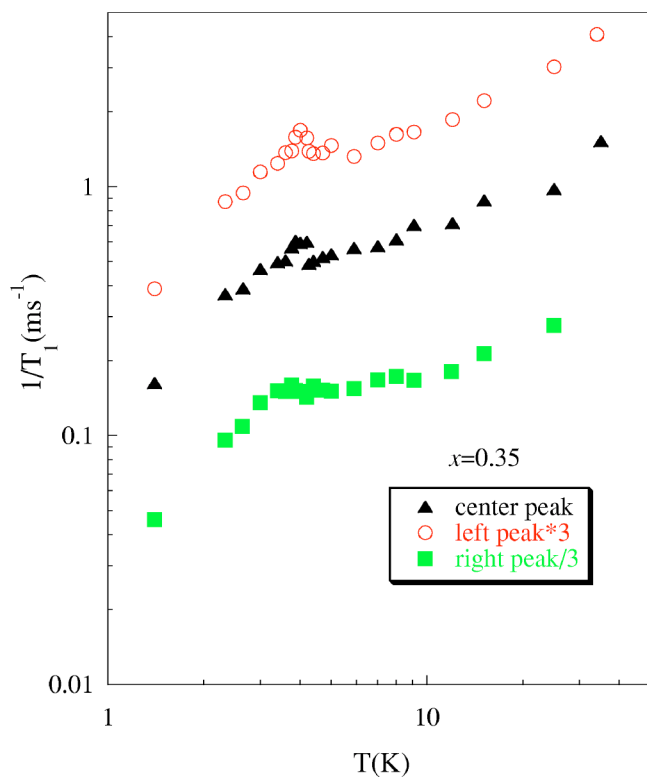

FIG. 6. (Color online) Temperature dependence of $1/T_1$ at the three $\pm3/2 \leftrightarrow \pm5/2$ transition lines of the In(2) site of $CeRh_{0.65}Ir_{0.35}In_5$. For clarity, $1/T_1$ at the left peak was multiplied by 3, while that for the right peak was divided by 3.

weaker than in the case of In(2), because In(1) is farther away from M. In addition, In(1) has eight nearest-neighbor M atoms. The effect of having different nearest-neighbor pair is thus further averaged out. As a result, each In(1) transition is observed as a broadened line. This is in contrast to the case of In(2) whose p-orbital directly mixes with those of M. Since ν_Q is dominated by the on-site electronic configuration,[25] the stronger coupling between In(2) and M atoms gives rise to three distinct resonance lines in the alloyed samples rather than a broad "single" transition as in the case of In(1). Although the In(2) transition is sensitive to the local atomic configuration, it should be emphasized that globally the electronic states are quite homogeneous, as evidenced by the results of spin-lattice relaxation measurements described in the next subsection.

B. Nuclear spin lattice relaxation and the magnetic ordering

The $1/T_1$ measurements were performed at the peak of the $2\nu_Q$ transition ($m = \pm3/2 \leftrightarrow \pm5/2$) for the In(1) site and at the central peak of the three lowest frequency transition ($m = \pm3/2 \leftrightarrow \pm5/2$) lines for the In(2) site. Figure 5 shows the decay curve of the nuclear magnetization for $x=0.45$ at three typical temperatures above and below T_N and T_c. At $T = 0.2$ K we used a small tipping-angle pulse so that the magnetization is less saturated at small delay time. The decay curve can be fitted by a single component of T_1 to the theoretical curve[22]

$$1 - \frac{M(t)}{M_0} = \frac{1}{33}\exp\left(-3\frac{t}{T_1}\right) + \frac{20}{143}\exp\left(-10\frac{t}{T_1}\right)$$
$$+ \frac{4}{165}\exp\left(-21\frac{t}{T_1}\right) + \frac{576}{715}\exp\left(-36\frac{t}{T_1}\right). \quad (4)$$

The same quality of data were obtained for all alloys and also for the In(2) site, whose nuclear magnetization is fitted to the theoretical curve[23] with a single component of T_1.
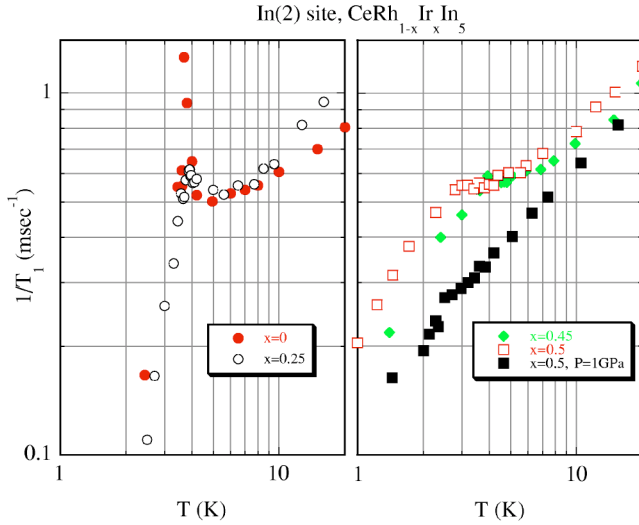
FIG. 7. (Color online) Typical data sets of $1/T_1$ measured at the central peak of the In(2) $\pm 3/2 \leftrightarrow \pm 5/2$ transition in CeRh$_{1-x}$Ir$_x$In$_5$.

$$1 - \frac{M(t)}{M_0} = 0.02421 \exp\left(-2.93355\frac{t}{T_1}\right)$$

$$+ 0.03961 \exp\left(-8.30137\frac{t}{T_1}\right)$$

$$+ 0.09771 \exp\left(-16.30355\frac{t}{T_1}\right)$$

$$+ 0.83847 \exp\left(-29.75056\frac{t}{T_1}\right). \qquad (5)$$

The successful fitting of the nuclear magnetization to the theoretical curve with a single T_1 component is a good indicator of the homogeneous nature of the electronic state. Figure 6 shows the temperature dependence of $1/T_1$ measured at the three peaks of In(2) for $x=0.35$. It can be seen that all sites show a quite similar T dependence. Namely, there is a peak around $T=4$ K, although the peak height is reduced as compared to $x=0.26$ The absolute value is also very similar. In the figure, the origin for the left and right peaks were shifted for clarity. These results indicate that the three peaks probe the same electronic state despite the fact that they arise from different nearest-neighbor M configurations.

Figure 7 shows the evolution of the T dependence of $1/T_1$ at the central In(2) transition for various Ir concentrations. It is evident that the peak temperature and the peak height change with the Ir concentration. We associate this peak with the Néel ordering temperature T_N at which $1/T_1$ increases due to critical slowing down. T_N determined in this manner correspond well with that inferred from the specific heat[11] and μsr measurements.[19] Interestingly, T_N first increases gradually with increasing Ir content up to $x=0.45$ then decreases rapidly. For $x=0.5$, T_N is reduced to 3 K. For $x=0.55$, no feature is seen in the T dependence of $1/T_1$ (for clarity of Fig. 7, data are not shown), thus it becomes difficult to identify T_N.

T_N inferred from the peak in $1/T_1$ is sensitive to externally applied hydrostatic pressure, as in pure CeRhIn$_5$. In the
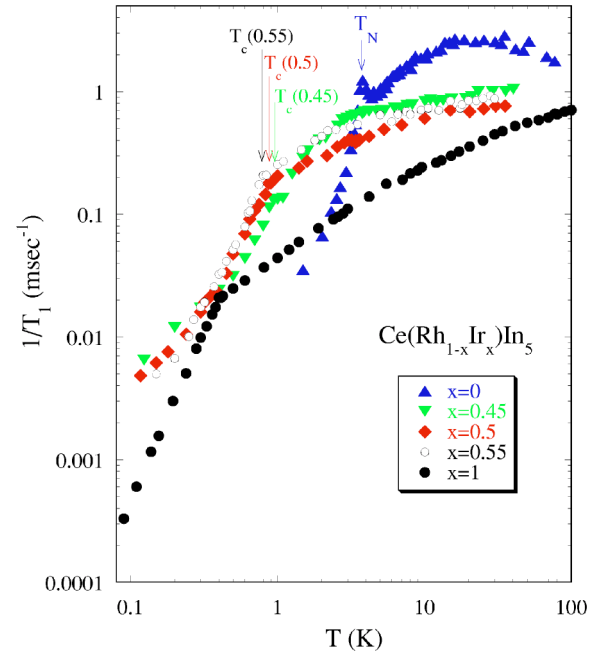

FIG. 8. (Color online) Typical data sets of ^{115}In $1/T_1$ measured at the In(1) site of CeRh$_{1-x}$Ir$_x$In$_5$. Data for $x=1$ and 0 are from Refs. 17, 26, and 27, respectively.

right panel of Fig. 7 is shown the T_1 result under a pressure of 1.02 GPa for the $x=0.5$ sample. The broad peak seen at ambient pressure is suppressed, and instead a distinct decrease of $1/T_1$ is found at 2.5 K, which resembles the case of pure CeRhIn$_5$ in which the application of pressure reduces the height of the peak at T_N (Refs. 26–29) and eventually suppresses the peak under $P=1.7$ GPa.[28] Thus, as in pure CeRhIn$_5$, T_1 can serve as a probe to determine T_N.

Figure 8 shows typical data sets of $1/T_1$ measured at the In(1) site. The anomaly at T_N is also visible at the In(1) site, although it is less clear presumably because the peak at T_N at this site is already rather weak, even in the undoped compound.

The nonmonotonic change of T_N as a function of x may be attributed to the increase of exchange coupling between $4f$ spins which is overcome by the increase of coupling between $4f$ spins and conduction electrons above $x=0.45$, as inferred from Doniach's treatment of the Kondo necklace.[30] This result also resembles the behavior of CeRhIn$_5$ (Refs. 13 and 14) as a function of pressure and indicates that the substitution of Ir for Rh acts as chemical pressure in CeRhIn$_5$.

Due to the broadening of the spectra upon alloying, it is difficult to estimate precisely the internal magnetic field in the ordered state. The Hamiltonion in the presence of magnetic field is given by

$$H = H_Q + H_{\text{Zeeman}}, \qquad (6)$$

where H_Q is given by Eq. (1) and

$$H_{\text{Zeeman}} = -\gamma\hbar(H_x I_x + H_y I_y + H_z I_z). \qquad (7)$$

In the present case, V_{zz} is along the crystal c axis. Assuming an internal magnetic field in the ab plane, which is the
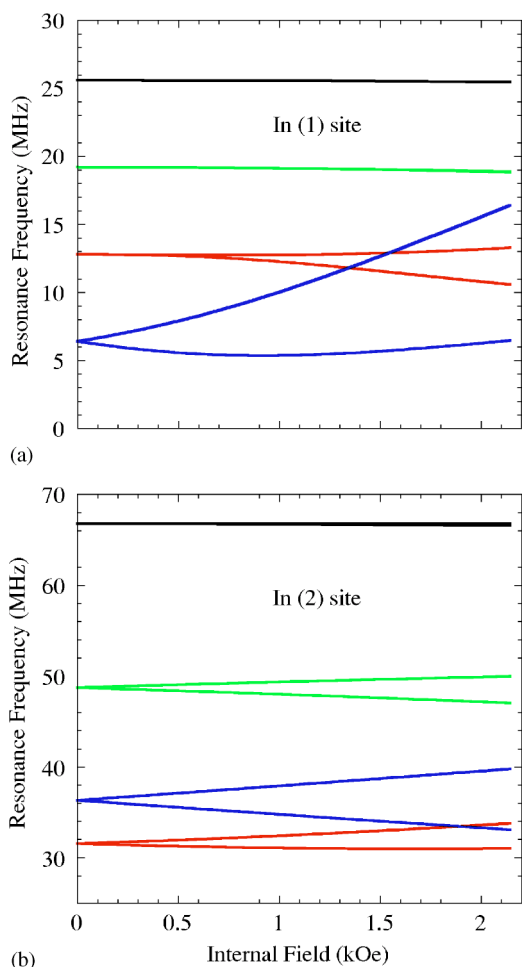
FIG. 9. (Color online) Calculated evolution of the NQR lines in the presence of internal field along the *a* axis for In(1) site (a) and In(2) site (b).

case for CeRhIn$_5$, the evolution of the resonance frequency for each transition is calculated for the In(1) site [Fig. 9(a)] and for the In(2) site [Fig. 9(b)]. Here, the field is assumed to be along the *x* direction. Note that even the *m* $=\pm3/2 \leftrightarrow \pm5/2$ transition for the In(2) site, which has a FWHM of 0.26 MHz and is the sharpest among all transitions in the alloyed samples, does not show an appreciable change between $T=4.2$ K (above T_N) and $T=1.4$ K (below T_N), see Fig. 10. This suggests that the internal magnetic field at the In(2) site is less than 200 Oe for $x=0.5$, as inferred from the expected splitting deduced from Fig. 9. Such a small internal field, which is samller by a factor of 10 than that in CeRhIn$_5$,[24] could be due to a moderate reduction of the ordered moment[31] with a concomitant reduction of the hyperfine coupling.[32]

C. Superconducting state

Next, we discuss the low temperature behavior of Ce(Rh$_{1-x}$Ir$_x$)In$_5$ well below T_N. Figure 11 shows $1/T_1$ for both the In(1) and In(2) sites at low temperatures for the x $=0.5$ sample. Below $T_c=0.9$ K, $1/T_1$ decreases sharply with no coherence peak, following a T^3 variation down to T
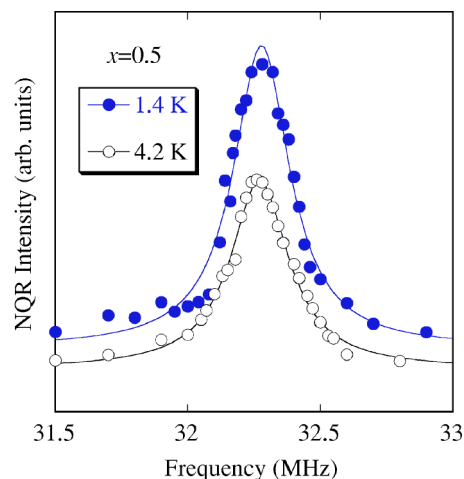

FIG. 10. (Color online) The central peak of the $\pm1/2 \leftrightarrow \pm3/2$ transition for CeRh$_{0.5}$Ir$_{0.5}$In$_5$ at $T=4.2$ and 1.4 K. For clarity, the horizon has been shifted.

$=0.45$ K. The observation of the T^3 behavior is strong evidence for the existence of line nodes in the superconducting gap function.[17] For an *s*-wave gap, $1/T_1$ would show a coherence peak just below T_c followed by an exponential decrease upon further decreasing T. Because $1/T_1$ is measured at the same transition for the entire measured temperature range, our results suggest that antiferromagnetic order and superconductivity are due to the same electronic state derived from the Ce-$4f^1$ electron. If the two ordered states occurred in spatially separated regions, the nuclear-magnetization decay curve would have been composed of two components (two T_1's) below T_N, contradicting the single-component decay curve we observe. It is noteworthy
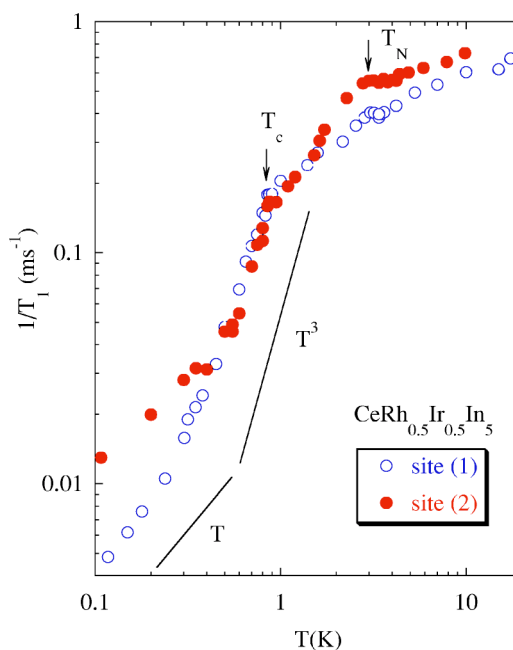

FIG. 11. (Color online) The $1/T_1$ results at low temperatures for CeRh$_{0.5}$Ir$_{0.5}$In$_5$ measured at the In(1) at In(2) sites, respectively. The two solid lines indicate the T^3 and *T*-linear variations, respectively.
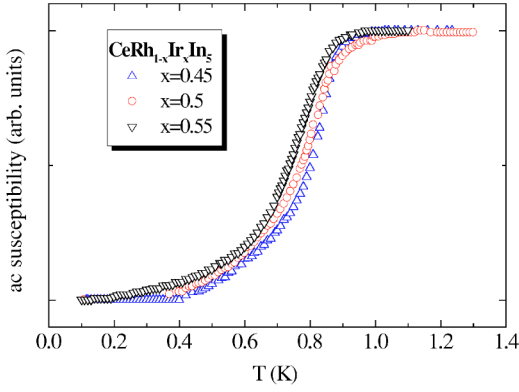
FIG. 12. (Color online) The ac susceptibility for $CeRh_{1-x}Ir_xIn_5$ ($x=0.45$, 0.5, and 0.55).

FIG. 13. (Color online) The normalized T_1 plotted against the reduced temperature for $CeRh_{1-x}Ir_xIn_5$ at the In(1) site. The solid curves are fits to the data as described in the text. N_r is for short of N_{res}/N_0.

that just above T_c, $1/T_1$ tends to be proportional to T, which suggests that there remains a finite density of states (DOS) at the Fermi level (E_F) in the magnetically ordered state, since $1/T_1T$ is dominantly proportional to the square of the low-energy DOS at such low-T [see below, Eq. (9)]. This suggests that the gap opening due to the antiferromagnetic order is incomplete, in contrast to the behavior observed in pure $CeRhIn_5$ where the gap is more fully developed, leading to a stronger decrease of $1/T_1$ (see Fig. 8). This remnant of some part of the Fermi surface may be important for superconductivity to set in even in the magnetically ordered state.

Finally, let us compare the superconducting behavior for $x=0.45$, 0.5, and 0.55. Figure 12 shows the ac susceptibility (ac-χ) measured using our NQR coil. Although it is hard to determine the onset temperature of the superconductivity from ac-χ, it can be seen that the midpoint of the transition increases in the order of $x=0.55$, 0.5, and 0.45. T_c determined from the point at which $1/T_1$ displays a distinct drop is 0.8, 0.9, and 0.94 K for $x=0.55$, 0.5, and 0.45, respectively. Figure 13 shows $1/T_1$ normalized by its value at T_c plotted against the reduced temperature T/T_c for $x=0.55$, 0.5, and 0.45. Just below T_c, $1/T_1$ shows identical behavior for all samples, but at lower temperatures strong variation is observed. In particular, below $T\sim 0.4$ K, $1/T_1$ becomes again proportional to T, and the normalized value of $1/T_1$ increases in the order $x=0.55$, 0.5, and 0.45.

The most straightforward explanation for T-linear $1/T_1$ at low T would be the presence of disorder that produces a finite DOS remaining at E_F. By assuming a gap function with line nodes

$$\Delta(\theta) = \Delta_0 \cos(\theta) \qquad (8)$$

and with a finite residual DOS, N_{res} (Ref. 33), we tried to fit the data in the superconducting state to

$$\frac{T_1(T=T_c)}{T_1} = \frac{2}{k_BT_c}\int\left(\frac{N_s(E)}{N_0}\right)^2 f(E)[1-f(E)]dE, \qquad (9)$$

where $N_s(E)/N_0=E/\sqrt{E^2-\Delta^2}$ with N_0 being the DOS in the normal state and $f(E)$ being the Fermi function. The resulting fitting parameters are $N_{res}/N_0=0.32$, 0.45, and 0.63 for $x=0.55$, 0.5, and 0.45, respectively, with $\Delta_0=2.5k_BT_c$ for all

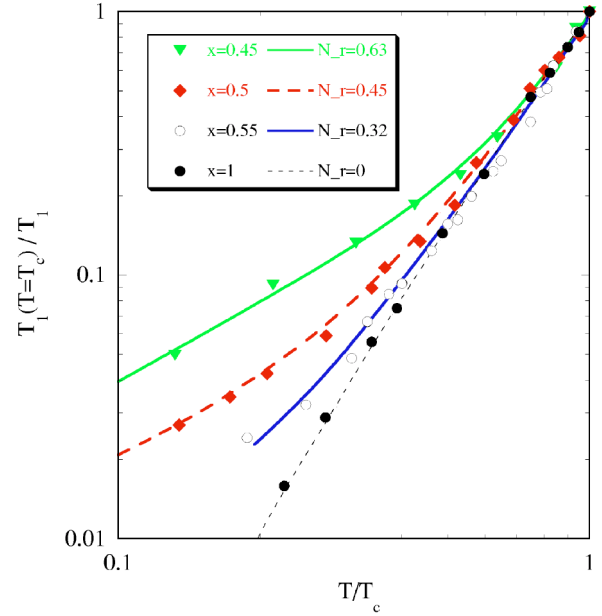samples. In such a case, however, one would expect N_{res} to be the same for $x=0.55$ and 0.45, because the amount of disorder is expected to be similar. The much larger N_{res} inferred for $x=0.45$ than $x=0.55$ suggests an additional mechanism. We propose that this additional N_{res} comes from low-lying magnetic excitations associated with the coexisting magnetic ordering that is more well developed at lower values of x. Similar N_{res} was seen in $CeRhIn_5$ under a pressure of 1.6 GPa where magnetism also coexists with superconductivity. In this case the observed behavior was interpreted as due to a gapless p-wave superconducting state,[34] or due to additional nodes in the d-wave order parameter.[35]

On the other hand, the larger N_{res} for the In(2) site than for In(1) site may be due to a larger disorder contribution for this site. This is because the source of disorder in the present case is in the Rh(Ir)In$_2$ block. The In(2) site is naturally more sensitive to such disorder than the In(1) site which is farther removed from this block. A similar case was seen in high-T_c copper oxide superconductors. In $Tl_2Ba_2Ca_2Cu_3O_{10}$ ($T_c=117$ K),[36] disorder due to intersubstitution of Ca/Tl occurs in the Ca layer. As a consequence, the Cu(1) site sandwiched by two Ca layers sees a larger N_{res} than the Cu(2) site which is adjacent to only one of the Ca layers.

D. Phase diagram

The phase diagram shown in Fig. 14 summarizes our results. Upon doping with Ir, the system undergoes a quantum phase transition from an antiferromagnet ($x=0$) to a superconductor ($x=1$), with an intervening region where antiferromagnetic and superconducting orders coexist. Our results show that this behavior, reported previously based on thermodynamic data,[11] is confirmed microscopically. T_c reaches
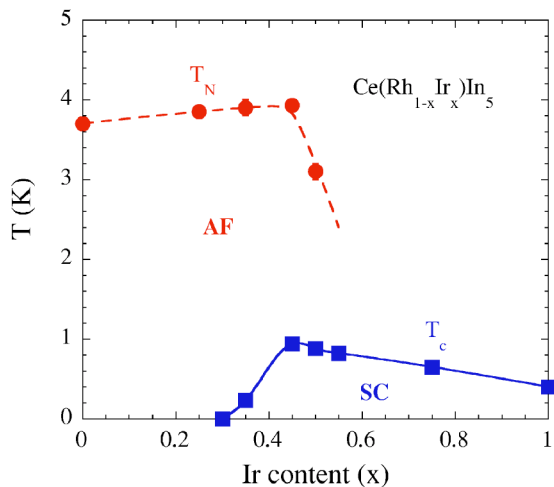
FIG. 14. (Color online) The phase diagram of $CeRh_{1-x}Ir_xIn_5$ obtained from NQR measurements. AF and SC mean antiferromagnetic and superconducting states, respectively.

a maximum at $x=0.45$ ($T_c=0.94$ K), while T_N is found to be the highest ($T_N=4.0$ K). The enhancement of T_c in the antiferromagnetically ordered state is most interesting, suggesting the importance of magnetism in producing the superconductivity. Recently, antiferromagnetism and superconductivity was found to coexist also in $CeRhIn_5$ under external pressures,[13,14] but the coexistent region is rather narrow there. More importantly, in the present case superconductivity develops well inside the ordered state and T_c increases when approaching the maximum of T_N, whereas T_c reaches a maximum after T_N disappears in hydrostatically pressurized $CeRhIn_5$. The observed phase diagram may be understood in the framework of SO(5) theory in which the five-component superspin can be rotated by a chemical potential from the subspace of antiferromagnetic order to the subspace of d-wave superconductivity and vice versa.[10] However, a microscopic description of how the same $4f^1$

electron can display both magnetic order and superconductivity is still lacking.

IV. CONCLUSION

In conclusion, we have carried out an extensive [115]In NQR study on $CeRh_{1-x}Ir_xIn_5$. We find that the substitution of Ir for Rh in the antiferromagnet $CeRhIn_5$ acts as chemical pressure. With increasing Ir content (x), T_N increases slightly up to $x=0.45$, then decreases rapidly. The coexistence of superconductivity with antiferromagnetism for $0.35 \leqslant x \leqslant 0.5$ is observed in the temperature dependence of $1/T_1$ which displays a broad peak at T_N and drops as T^3 below T_c. At $x=0.5$, T_N is reduced to 3 K while T_c reaches 0.9 K. Our results suggest that the coexisting antiferromagnetic order and superconductivity are due to the same electronic state derived from the Ce-$4f^1$ electron. It is most interesting that the superconducting transition temperature T_c is increased as the system penetrates deeper inside the antiferromagnetically ordered state. T_c for $x=0.45$ and 0.5 is more than double that of $CeIrIn_5$. In the coexistence region, $1/T_1$ shows a T-linear dependence at low-T below $T \sim 0.4$ K. We have argued that this may arise from some magnetic excitations associated with the coexisting magnetism, in addition to the presence of crystal disorder that produces a residual density of states at the Fermi level.

*Present address: Department of Physics, Okayama University, Okayama 700-8530, Japan. Email address: zheng@psun.phys.okayama-u.ac.jp

[1] *Superconductivity and Magnetism*, edited by M. B. Maple and O. Fisher (Springer-Verlag, Berlin, 1982).

[2] C. Bernhard, J. L. Tallon, E. Bruher, and R. K. Kremer, Phys. Rev. B **61**, R14 960 (2000).

[3] C. Geibel, C. Shank, S. Thies, H. Kitazawa, C. D. Bredl, A. Bohm, M. Rau, A. Grauel, R. Caspary, R. Hefrich, R. Ahlheim, G. Weber, and F. Steglich, Z. Phys. B: Condens. Matter **84**, 1 (1991).

[4] H. Tou, Y. Kitaoka, K. Asayama, C. Geibel, C. Shank, and F. Steglich, J. Phys. Soc. Jpn. **64**, 725 (1995).

[5] N. K. Sato, N. Aso, K. Miyake, R. Shiina, P. Thalmeier, G. Varelogiannis, C. Geibel, F. Steglich, P. Fulde, and T. Komatsubara, Nature (London) **410**, 340 (2001).

[6] S. Yotsuhashi, H. Kusunose, and K. Miyake, J. Phys. Soc. Jpn.

70, 186 (2001).

[7] C. Geibel, S. Thies, D. Kaczorowski, A. Mehner, A. Grauel, B. Seidel, U. Ahlheim, R. Helfrich, K. Petersen, C. D. Bredl, and F. Steglich, Z. Phys. B: Condens. Matter **83**, 305 (1991).

[8] S. S. Saxena, P. Agarwal, K. Ahilan, F. M. Grosche, R. K. W. Haselwimmer, M. J. Steiner, E. Pugh, I. R. Walker, S. R. Julian, P. Monthoux, G. G. Lonzarich, A. Huxley, I. Sheikin, D. Braithwaite, and J. Flouquet, Nature (London) **406**, 587 (2000).

[9] D. Aoki, A. Huxley, E. Ressouche, D. Braithwaite, J. Flouquet, J. P. Brison, E. Lhotel, and C. Paulsen, Nature (London) **413**, 613 (2001).

[10] S.-C. Zhang, Science **275**, 1089 (1997).

[11] P. G. Pagliuso, C. Petrovic, R. Movshovich, M. F. Hundley, J. L. Sarrao, J. D. Thompson, and Z. Zisk, Phys. Rev. B **64**, 100503(R) 2001).

[12] V. S. Zapf, E. J. Freeman, E. D. Bauer, J. Petricka, C. Sirvent, N. A. Frederick, R. P. Dickey, and M. B. Maple, Phys. Rev. B **65**,

014506 (2002).

[13] T. Mito, S. Kawasaki, Y. Kawasaki, G.-q. Zheng, Y. Kitaoka, D. Aoki, Y. Haga, and Y. Onuki, Phys. Rev. Lett. **90**, 077004 (2003).

[14] S. Kawasaki, T. Mito, Y. Kawasaki, G.-q. Zheng, Y. Kitaoka, D. Aoki, Y. Haga, and Y. Onuki, Phys. Rev. Lett. **91**, 137001 (2003).

[15] H. Hegger, C. Petrovic, E. G. Moshopoulou, M. F. Hundley, J. L. Sarrao, Z. Fisk, and J. D. Thompson, Phys. Rev. Lett. **84**, 4986 (2000).

[16] C. Petrovic, R. Movshovich, M. Jaime, P. G. Pagliuso, M. F. Hundley, J. L. Sarrao, Z. Fisk, and J. D. Thompson, Europhys. Lett. **53**, 354 (2001).

[17] G.-q. Zheng, K. Tanabe, T. Mito, S. Kawasaki, Y. Kitaoka, D. Aoki, Y. Haga, and Y. Onuki, Phys. Rev. Lett. **86**, 4664 (2001).

[18] W. Bao, G. Aeppli, J. W. Lynn, P. G. Pagliuso, J. L. Sarrao, M. F. Hundley, J. D. Thompson, and Z. Fisk, Phys. Rev. B **65**, 100505 (2002).

[19] G. D. Morris, R. H. Heffner, J. E. Sonier, D. E. MacLaughlin, O. O. Bernal, G. J. Nieuwenhuys, A. T. Savici, P. G. Pagliuso, and J. L. Sarrao, Physica B **326**, 390 (2003).

[20] G.-q. Zheng, E. Yanase, Y. Kitaoka, K. Asayama, Y. Kodama, R. Tanaka, and S. Endo, Solid State Commun. **79**, 51 (1991).

[21] T. F. Smith, C. W. Chu, and M. B. Maple, Cryogenics **9**, 53 (1969).

[22] D. E. MacLaughlin, J. D. Williamson, and J. Butterworth, Phys. Rev. B **4**, 60 (1971).

[23] J. Chepin and J. H. Ross, J. Phys.: Condens. Matter **3**, 8103 (1991).

[24] N. J. Curro, P. C. Hammel, P. G. Pagliuso, J. L. Sarrao, J. D. Thompson, and Z. Fisk, Phys. Rev. B **62**, R6100 (2000).

[25] K. Betsuyaku and H. Harima, J. Magn. Magn. Mater. **272–276**, 187 (2004).

[26] T. Mito, S. Kawasaki, G.-q. Zheng, Y. Kawasaki, K. Ishida, Y. Kitaoka, D. Aoki, Y. Haga, and Y. Onuki, Phys. Rev. B **63**, 220507 (2001).

[27] S. Kawasaki, T. Mito, G.-q. Zheng, C. Thessieu, Y. Kawasaki, K. Ishida, Y. Kitaoka, D. Aoki, S. Araki, Y. Haga, R. Settai, and Y. Onuki, Phys. Rev. B **65**, 020504 (2002).

[28] T. Mito *et al.* (unpublished).

[29] Y. Kohoria, Y. Yamato, Y. Iwamoto, and T. Kohara, Eur. Phys. J. B **18**, 601 (2000).

[30] S. Doniach, in *Valence Instabilities and Related Narrow Band Phenomena*, edited by R. D. Parks (Plenum, New York, 1977), p. 169.

[31] Preliminary neutron results suggest that the ordered moment for $x=0.5$ is reduced by a factor of 4 from that for the $x=0$ sample [A. D. Christianson (private communication)].

[32] In fact, on going from $CeRhIn_5$ to $CeCoIn_5$, the hyperfine coupling decreases by a factor of 3. See Curro *et al.*, cond-mat/0205354 (unpublished).

[33] S. Schmitt-Rink, K. Miyake, and C. M. Varma, Phys. Rev. Lett. **57**, 2575 (1986); K. Miyake (unpublished).

[34] Y. Fuseya, H. Kohno, and K. Miyake, J. Phys. Soc. Jpn. **72**, 2914 (2003).

[35] Y. Bang, M. J. Graf, A. V. Balatsky, and J. D. Thompson, Phys. Rev. B **69**, 014505 (2004).

[36] G.-q. Zheng, Y. Kitaoka, K. Asayama, K. Hamada, H. Yamauchi, and S. Tanaka, Physica C **260**, 197 (1996).